



Hydrogen-Bonded Organic Semiconductors with Long Charge Carrier Lifetimes

Nelson Ricardo Ávila Roveló, Gabriel Martinez, Wakana Matsuda, Stephan Sinn,
Patrick Lévêque, Duncan Schwaller, Philippe Mesini, Shu Seki, Amparo
Ruiz-Carretero

► To cite this version:

Nelson Ricardo Ávila Roveló, Gabriel Martinez, Wakana Matsuda, Stephan Sinn, Patrick Lévêque, et al.. Hydrogen-Bonded Organic Semiconductors with Long Charge Carrier Lifetimes. *Journal of Physical Chemistry C*, 2022, 126 (26), pp.10932-10939. <10.1021/acs.jpcc.2c03105>. <hal-03847365>

HAL Id: hal-03847365

<https://hal.science/hal-03847365v1>

Submitted on 10 Nov 2022

HAL is a multi-disciplinary open access archive for the deposit and dissemination of scientific research documents, whether they are published or not. The documents may come from teaching and research institutions in France or abroad, or from public or private research centers.

L'archive ouverte pluridisciplinaire **HAL**, est destinée au dépôt et à la diffusion de documents scientifiques de niveau recherche, publiés ou non, émanant des établissements d'enseignement et de recherche français ou étrangers, des laboratoires publics ou privés.



HAL Authorization

Hydrogen-bonded organic semiconductors with long charge carrier lifetime

Nelson Ricardo Ávila-Rovelo,^[a] # Gabriel Martínez,^[a]# Wakana Matsuda,^[b] Stephan Sinn^[c], Patrick Lévêque,^[d] Duncan Schwaller,^[a] Philippe Mésini,^[a] Shu Seki,^[b] and Amparo Ruiz-Carretero^{*[a]}

Affiliations:

^[a]Nelson Ricardo Ávila Rovelo, Gabriel Martínez, Duncan Schwaller, Dr. Philippe Mésini, Dr. Amparo Ruiz Carretero. University of Strasbourg, Institute Charles Sadron, CNRS, UPR22, 23 Rue du Loess, 67034, Strasbourg Cedex 2, France.

E-mail: amparo.ruiz@ics-cnrs.unistra.fr

^[b]Dr. W. Matsuda, Prof. S. Seki. Department of Molecular Engineering, Graduate School of Engineering, Kyoto University, Nishikyo-ku, Kyoto 615-8510, Japan.

^[c]Dr. Stephan Sinn. Karlsruhe Institute of Technology (KIT), Institute of Nanotechnology, Hermann-von-Helmholtz-Platz. 76344 Eggenstein-Leopoldshafen, Germany.

^[d]Dr. Patrick Lévêque. Le laboratoire des sciences de l'ingénieur, de l'informatique et de l'imagerie (ICube), UMR7357, Université de Strasbourg-CNRS, 23 rue du Loess, 67037 Strasbourg, France.

#Equal contribution

Abstract

Hydrogen bonds are noncovalent interactions able to improve the electronic properties of self-assembled semiconductors. Nevertheless, it is necessary to control the parameters influencing the formation of hydrogen bonds to achieve hierarchical structures with enhanced properties. In this work, we explore two hydrogen-bonded thiophene-capped diketopyrrolopyrrole (DPP) derivatives containing amides with different topology (C- or N-centered), and compare them to a control analogue without hydrogen bonds. We demonstrate the differences in the optoelectronic and self-assembly properties of the two amide-containing DPP derivatives, as well as in their charge carrier lifetimes. We prove the superior properties of the hydrogen-bonded derivatives in comparison to the control molecule without hydrogen bonds, and show that our molecular design strategy results in supramolecular structures with

particularly long charge carrier lifetime compared to other amide-containing semiconductors reported in literature.

Introduction

Supramolecular electronic materials have been widely studied in the last decades due to the exciting properties they have thanks to the interplay of noncovalent interactions.¹⁻³ The arrangement of π -conjugated materials is directed towards well-defined assemblies where not only the structures are improved, but also the properties^{4,5}. Particularly, hydrogen bonds (H-bonds) are noncovalent interactions demonstrated to increase the efficiency of different electronic devices.⁶⁻⁸ Nevertheless, their use has been overlooked because the fabrication of electronic devices implies the optimization of multiple parameters, resulting in a large combinatorial space. This turns into a very tedious task when implementing new materials, as for instance, H-bonded molecules. This usually leads to a lack of consensus regarding their incorporation into electronic devices.^{9,10} Still, the proper control of the H-bonded semiconducting structures opens a strategy for the design of alternative organic electronic materials whose properties can be modified through aggregation. Our group and others have studied H-bonded π -conjugated molecules containing different H-bonding functionalities, such as semicarbazones,¹¹ ureas,¹²⁻¹⁴ amides¹⁵⁻¹⁹ or self-complementary H-bonds²⁰⁻²² to explore the impact of H-bonding in the optoelectronic properties of the assemblies. Amide functionalities are among the best-known H-bonding forming groups,²³ being the amide topology (N- or C- centered) a subtle, but very important parameter able to change the self-assembly of a given system and hence, the properties.^{24,25}

In this work, we show amide-containing thiophene-capped diketopyrrolopyrrole (DPP) derivatives with different amide topology to investigate its influence on the self-assembly, optoelectronic and charge transport properties. We compare two DPP derivatives containing amide groups with N- or C-centered topology, attached to the lactams through flexible alkyl linkers. To provide solubility, we have added hexyl tails to the thiophene in the extremities of the molecule (Scheme 1). Furthermore, we have also synthesized a DPP molecule having only hexyl alkyl tails in the lactams and the thiophenes as a control. We chose DPP²⁶⁻²⁹ as the π -conjugated segment due to its interesting electronic properties and the different positions available for functionalization. We have already explored other families of H-

bonded DPP with different H-bonding functionalities^{30,31} to have an overall picture of the role of H-bonds in the optoelectronic properties of DPP supramolecular systems. In this work, we follow the self-assembly processes of the N- and C-centered amide-containing DPP derivatives with different spectroscopy and microscopy techniques, and study the charge transport properties with a contactless technique based on dielectric microwave conductivity. The differences in aggregation and morphology between the two topology amides are discussed, as well as compared to the control molecule not containing H-bonds. Furthermore, we compare the charge transport results of the amide-containing DPPs to the control molecule and to previously reported H-bonded derivatives measured with the same contactless technique. We evaluate the recombination lifetime of the three derivatives and discuss the results according to the molecular design. With our results, we expect to provide new strategies for the design of H-bonded semiconductors with enhanced properties.

Methods

All reagents and solvents were obtained from commercial suppliers and purified or dried according to standard procedures. Column chromatography was performed on silica gel (VWR Silica 60, particle size 0.040–0.063 mm). Solvents for spectroscopic studies were of spectroscopic grade and used as received. Elemental analysis was performed on a Thermofischer Scientific Flash 2000. Matrix-assisted laser desorption/ionisation-time of flight (MALDI) was performed in a Bruker Daltonics. ¹H and ¹³C spectra were recorded in CDCl₃ on a Bruker Avance 400 MHz spectrometer and/or Bruker Avance III HD 500 MHz spectrometer. UV–vis measurements were performed in a conventional quartz cell (light pass 1 mm) on a Cary 5000 UV-Vis-NIR spectrophotometer. TEM measurements were done with a Technai G2 (FEI) microscope with an accelerating voltage of 200 kV. 5 µL of the sample solution were deposited onto a freshly glow discharged carbon-covered grid (400 mesh). The suspension was left for 2 min, and then, the grid was negatively stained with 5 µL of uranyl acetate (2% in water) for another 1 min and finally blotted using a filter paper.

FTIR spectra were recorded with a Vertex 70 from Bruker Optics, equipped with MCT detector and a black-body source. The spectra of the solids were measured by ATR on diamond.

Charge carrier mobilities were evaluated by FP-TRMC at room temperature. The thin films of samples were fabricated by drop-cast method onto quartz substrates ($9 \times 40 \text{ mm}^2$, 1 mm thick). Charge carriers were injected into the materials via photo-ionization with a third harmonic generation ($\lambda = 355 \text{ nm}$) of a Spectra Physics model INDI-HG Nd:YAG laser pulses at 10 Hz with a pulse duration of ca. 5 ns. The photon density of a 355 nm pulse was modulated from $9.1 \times 10^{15} \text{ photons cm}^{-2} \text{ pulse}^{-1}$. The microwave frequency and power were set at $\sim 9.1 \text{ GHz}$ and 3 mW, respectively, and guided into a microwave cavity. The Q -factor of the microwave cavity loaded with the sample was 2200, and the substrates with the compound films were set at the point of electric field maximum. The reflected power of the probing microwave, picked up by a diode (rise time $< 1 \text{ ns}$), was monitored by a Tektronics model TDS3032B digital oscilloscope after an amplification by Ciao Electronics CA812-304 FET amplifier system. The observed change in the reflected microwave power (ΔP_r) was normalised with the steady reflection of the microwave from the cavity (P_r), and converted directly into the product of a photocarrier generation yield (ϕ) and the sum of photo-generated electron/hole mobilities ($\Sigma\mu$),

$$\phi\Sigma\mu = 1/(\varepsilon I_0 F_{\text{light}}) \times (1/A) \times (\Delta P_r/P_r), \quad (1)$$

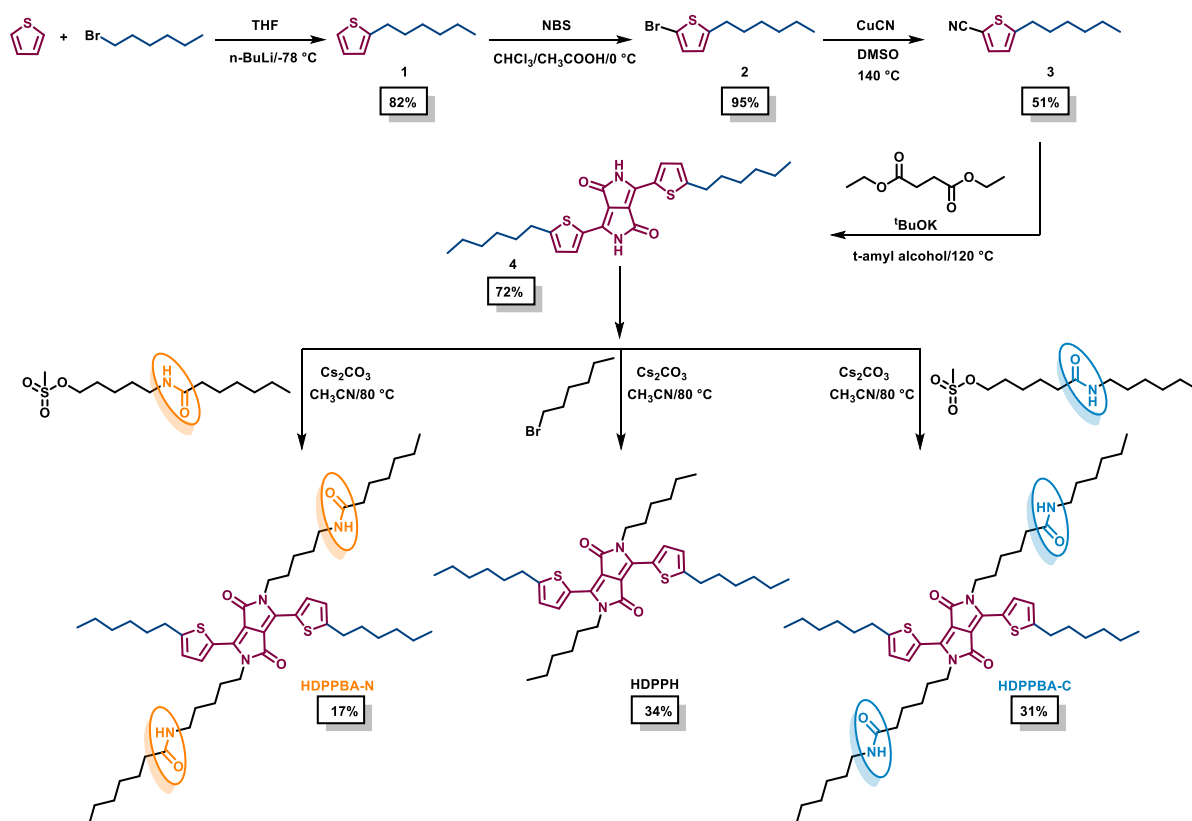
where ε , A , I_0 , and F_{light} are elementary charge, sensitivity factor ($\text{S}^{-1} \text{ cm}$), incident photon density of the excitation laser (photon cm^{-2}), and filling factor (cm^{-1}), respectively. The value of F_{light} was calculated based on the overlap of the area of photo-carrier injection (presumed to be proportional to the absorbance of excitation light by the sample film) with electric field strength distribution in the cavity derived from a calculation code of CST Microwave Studio from AET Inc.

Results and Discussion

Synthesis

HDPPBA-C and **HDPPBA-N** were synthesized following a convergent approach (Scheme 1) starting with the functionalization of the thiophene ring and finalizing with a cyclization reaction to form the DPP core. Initially, the thiophene ring was alkylated with hexyl bromide (**1**) in high yield, and subsequently, a nitrile group was introduced in position 5 after replacement of a bromine atom (Scheme

1). Then 5-hexylthiophene-2-carbonitrile (**3**) reacted with diethylsuccinate in the presence of potassium *t*-butoxide to form the hexyl-functionalized thiophene-capped DPP main core (**4**) in 72% yield. In a last step, the lactam rings of the DPP were alkylated with the amide-containing branches that were synthesized in parallel. The mesylated carbon-centered amide (-CONH) branch was synthesized following a synthetic route previously described in the literature.¹⁷ It involves the reaction between ϵ -caprolactone with hexylamine and subsequently adding the mesylate activating group (Scheme S1). On the other hand, Schotten-Baumann conditions were followed to obtain the N-centered amide (-NHCO) branch (Scheme S2). In this case the acylation of 5-amino-1-pentanol with heptanoyl chloride was carried out in a biphasic system of dichloromethane and a basic aqueous solution. The use of base drives the equilibrium of the reaction towards the formation of the amide, obtained in high yield. Next, the N-centered amide was treated with methanesulfonyl chloride to achieve the mesylated amide-containing branch (Scheme S2). The last step was the alkylation of the DPP core functionalized with hexyl tails in the thiophenes with the amide-containing branches. In this case, we replaced *N,N*-dimethylformamide (DMF), which is the most commonly employed solvent, by acetonitrile, a greener solvent that allows lowering the reaction temperature and time, as well as the need of dry solvent and inert atmosphere.³² The purification and isolation of the final product was straightforward since we did not obtain *N,O*- and/or *O,O'*- alkylated isomers, which are common side products of this reaction. In this sense, the starting material (**4**) seems to provide higher regioselectivity towards the *N,N'*-alkylated product. It might be explained by the improved solubility of the starting material (introduction of hexyl groups in the thiophene *vs* previously reported DPP without functionalization in the thiophenes¹⁷), the steric hindrance provided by the hexyl chains with respect to the DPP carbonyl groups, the lower reaction temperature (80 °C in CH₃CN *vs* 120 °C in DMF) and the choice of base (cesium carbonate *vs* potassium carbonate). The improved regioselectivity resulted in higher yields for the alkylation reactions in the lactams, reaching 30% in comparison to the same reaction using non-alkylated thiophene-capped DPP derivatives reported earlier by our group.¹⁷ The control molecule **HDPPH** was synthesized following the same strategy but the lactam rings were alkylated with hexyl bromide (Scheme S3). All the derivatives were characterized with proton and carbon nuclear magnetic resonance (¹H and ¹³C-NMR), and mass spectrometry (all the details can be found in the Supporting Information).



Scheme 1. Synthetic route towards **HDPPBA-C** and **HDPPBA-N**

Self-assembly and optical properties, and morphology

The optical and self-assembly properties of **HDPPBA-C**, **HDPPBA-N** and **HDPPH** were followed by UV-Vis absorption at variable temperature in different solvents and concentrations, and Fourier transform infrared (FTIR) spectroscopy. The amide-containing derivatives as well as the control molecule display broad absorption bands ranging from 400 to 600 nm at $20\text{ }^{\circ}\text{C}$ in chloroform with absorption maxima at $\lambda = 521\text{ nm}$ and $\lambda = 560\text{ nm}$ (Figure S1). The three derivatives do not show any sign of aggregation in chloroform at $20\text{ }^{\circ}\text{C}$ at 0.5 mg/ml , and the absorption bands do not change upon heating or changing the concentration (Figure S2 a-f). Additional absorption bands appeared at lower energy when **HDPPBA-C** and **HDPPBA-N** were measured in different solvents, such as chlorobenzene, toluene and ethyl acetate at the same concentration (Figure 1a and 1b) with λ_{max} at 620 nm in chlorobenzene and toluene, and at 630 nm in ethyl acetate for **HDPPBA-C**, and λ_{max} at 617 nm in chlorobenzene, 620 nm in toluene and 624 nm in ethyl acetate for **HDPPBA-N**. Interestingly, this band

at lower energy was not observed for the control molecule **HDPPH**, which displayed equal spectra in all the solvents (Figure 1c). When comparing to previously described amide-containing DPPs in our group,¹⁷ where the α -position of the thiophene was not functionalized with hexyl tails, a bathochromic shift of 10 nm of the J-aggregate band was observed.

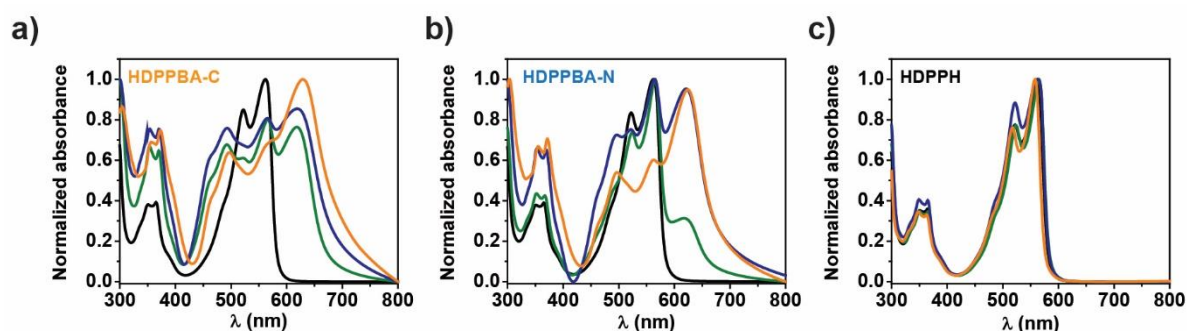


Figure 1. Absorption spectra of a) **HDPPBA-C**, b) **HDPPBA-N** and c) **HDPPH** at room temperature in different solvents (chloroform, black traces; chlorobenzene, green traces; toluene, blue traces, and ethyl acetate, orange traces). $[\text{HDPPBA-C}] = [\text{HDPPBA-N}] = [\text{HDPPH}] = 0.5 \text{ mg/ml}$.

The additional bands above 600 nm are attributed to the formation of J-type aggregates, as detected for the other families of H-bonded DPPs previously described by us and other groups.^{14,17,18,30,33} Furthermore, the differences found between the amide derivatives and the control suggest that H-bonds are involved in the formation of such types of aggregates. To confirm this hypothesis, the absorption spectra were measured after the addition of methanol, an H-bonding competing solvent, showing that the J-aggregate bands disappear (Figure S3).

Both **HDPPBA-C** and **HDPPBA-N** display aggregate bands not present in the control molecule, but differences between them were also observed. **HDPPBA-C** presents a bathochromic shift of the main absorption and aggregate bands in all the solvents compared to **HDPPBA-N**. In addition, the aggregate bands are more pronounced for the C-centered amide, as a consequence of stronger aggregation for this derivative compared to the N-centered. This effect could be observed by the naked eye since solutions of both amide derivatives in the same solvent and concentration, have different colors (Figure S4). Furthermore, the disappearance of the J-aggregate band was observed either upon diluting (Figure S5 a-b) or heating in all the solvents studied (Figure S5 c-d). For **HDPPBA-C**, the J-aggregate band was

observed at lower concentrations than for **HDPPBA-N** and it was present at higher temperatures (Figure S5)

FTIR spectra of powders at room temperature further confirm the existence of H-bonds in the bisamide derivatives. **HDPPBA-C** and **HDPPBA-N** showed a band at 3303 cm^{-1} assigned to the NH stretching bands of the amides. This frequency shows the amides are H-bonded³⁴ (Figure S6). In the region between 1600 cm^{-1} and 1700 cm^{-1} , the amide derivatives and the control show peaks at 1655 cm^{-1} , corresponding to the amide I bands of the lactam rings of the DPP core. In the same area, the other peaks at 1641 cm^{-1} and 1637 cm^{-1} for **HDPPBA-C** and **HDPPBA-N** respectively, correspond to amide groups engaged in H-bonding (Figure S6). The amide II bands are located at 1550 cm^{-1} and 1548 cm^{-1} for **HDPPBA-C** and **HDPPBA-N** respectively, which also shows the amide groups are H-bonded. These large bands overlap with the amide II band of the lactam, visible at 1553 cm^{-1} for **HDPPH**. The difference of 4 cm^{-1} between the amide-containing derivatives indicates a slight difference in the strength of the H-bonds that can induce subtle differences in aggregation.

Ground state Density-functional theory (DFT) calculations of the individual molecules in the gas phase were performed to rationalize the behavior of the amide-containing derivatives. DFT calculations were carried out utilizing the hybrid functional B3LYP with the standard valence basis set 6-31G(d,p) for C, H, N and O. The found stationary points possess no imaginary frequencies and therefore, assumed to be true minima. All calculations were performed with the program package G16.C.01.³⁵ The results display differential dihedral angles for **HDPPBA-C** and **HDPPBA-N**, being that the N-centered derivative more similar to the control molecule (Figure 2). **HDPPH** is quite planar, with angles between the DPP core and the thiophenes of 5° and 15° , similar to **HDPPBA-N**, which has angles of 0° and 20° . In contrast, the C-centered derivative is the least planar of the three, with both angles of 20° . As expected, the frontier orbitals are in any case strongly located at the conjugated DPP core featuring similar HOMO-LUMO gaps of around $2.51 (\pm 0.02)\text{ eV}$, which agrees with the optical energy band gaps calculated from the absorption spectra in chloroform for the three derivatives. Nevertheless, the optical band gaps are narrower for the H-bonded derivatives in self-assembling promoting solvents, such as chlorobenzene and toluene, ranging from $2\text{--}1.66\text{ eV}$ for **HDPPBA-C** and of $1.98\text{--}1.61\text{ eV}$ for **HDPPBA-N**, depending on the concentration (1-0.03 mg/ml).

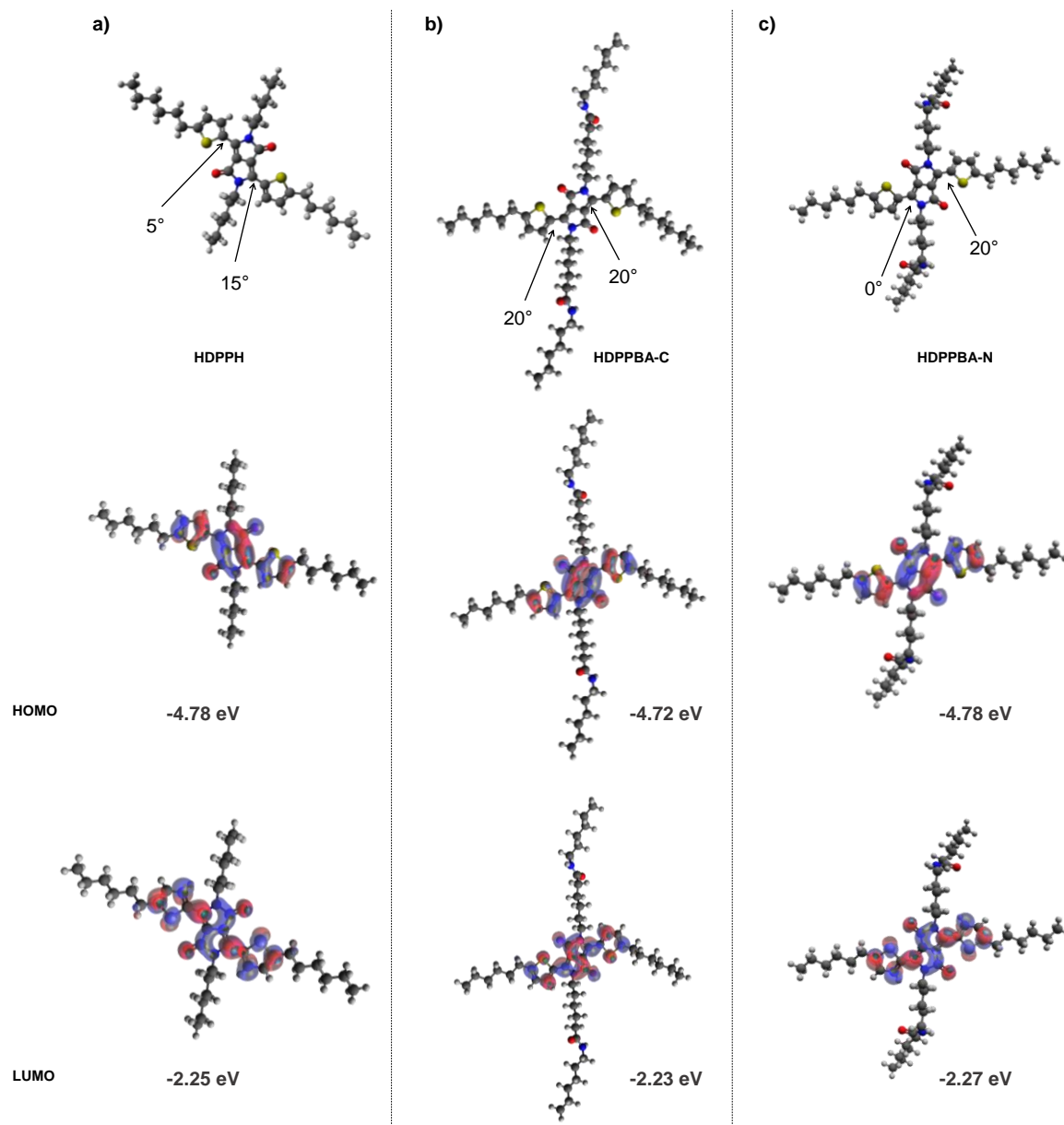


Figure 2. Geometry-optimized DFT models including the dihedral angle measurements. Kohn-Sham orbitals of the frontier orbitals of the ground-state configuration of the molecules comprising the corresponding energetic levels. a) **HDPPH**; b) **HDPPBA-C**, c) **HDPPBA-N**.

The morphology of **HDPPBA-C**, **HDPPBA-N** and **HDPPH** was studied using TEM in different solvents (Figure 3). Clear differences were found when comparing the H-bonded derivatives to the control molecule. While **HDPPBA-C** and **HDPPBA-N** self-assemble into high aspect-ratio structures, **HDPPH** forms short tape-like crystallites of approximately 2 μm in length overlapping with each other

in all the solvents tested (Figure 3k-n) except for cyclohexane, where the tape-like structures are narrower and longer (Figure 3o). In the case of **HDPPBA-C**, a great disparity of fibers with different width and length were observed in toluene, ethyl acetate and cyclohexane (Figure 3b-e). In toluene, the fibers are wavy, intertwined in bundles of rectangular size, and their length can exceed 15 μm (Figure 3b). The structures in chlorobenzene are slightly different, finding elongated fibers as well, but narrower, less twisted than in the other solvents and with sharper edges (Figure 3c). In chloroform, there are much smaller fibers that are straight and flat. These are the usual structures observed for the other DPP derivatives we have studied so far in chloroform and it seems to be in part due to drying effects (Figure 3a). The structures found in ethyl acetate and cyclohexane are very similar (Figure 3d-e), finding tape-like structures with well-defined edges. Regarding **HDPPBA-N** the structures observed are different from those of **HDPPBA-C**, finding very similar fibers in all the solvents except for in chloroform (Figure 3g-j). Elongated fibers up to 5 μm were found, but generally smaller than those of **HDPPBA-C**. They are wavy and twisted fibers they appear to be folded into several thin layers. In the case of chloroform, the fibers are very different and in some areas of the sample, they resemble the fibers found in **HDPPBA-C** (Figure 3f).

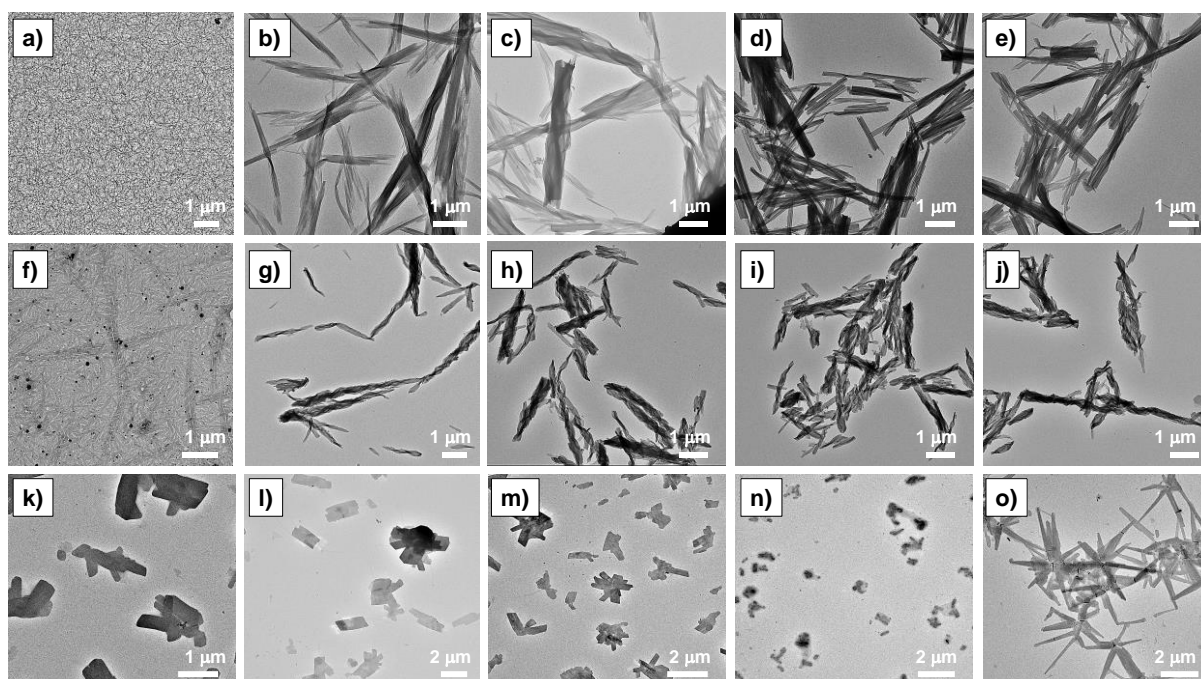


Figure 3. TEM images of **HDPPBA-C** (a-e), **HDPPBA-N** (f-j) and **HDPPH** (k-o) in chloroform, chlorobenzene, toluene, ethyl acetate and cyclohexane, respectively.

Electrical measurements: Flash photolysis time-resolved microwave conductivity (FP-TRMC)

The photoconductivity properties of **HDPPBA-C**, **HDPPBA-N** and the control molecule were measured by flash photolysis-time resolved microwave conductivity (FP-TRMC) upon irradiation with a 355 nm pulsed laser. FP-TRMC is a contactless technique that affords a measure of photoconductivity as $\Phi\Sigma\mu$ where Φ is the charge carrier generation quantum yield and $\Sigma\mu$ is the sum of charge carrier mobilities (electrons and holes). Thin films of the compounds were prepared by drop casting from chloroform/toluene solutions, and their photoconductivity was directly analysed. The kinetic traces of conductivity transients can be seen in figure 4a. Despite the differences found in aggregation, the photoconductivity values of **HDPPBA-C** and **HDPPBA-N** are very similar, being of $2.0 \times 10^{-5} \text{ cm}^2\text{V}^{-1}\text{s}^{-1}$ and $1.6 \times 10^{-5} \text{ cm}^2\text{V}^{-1}\text{s}^{-1}$ respectively (Table 1, entries 1 and 2) when measuring up to 10 μs . Interestingly, these values are clearly larger than the value found for **HDPPH**, being of $5.8 \times 10^{-6} \text{ cm}^2\text{V}^{-1}\text{s}^{-1}$ (Table 1, entry 3), which is one order of magnitude smaller than for the H-bonded derivatives. The kinetic decays of photoconductivity of **HDPPBA-C** and **HDPPBA-N** showed that the photogenerated free charge carriers are stable for more than 10 μs , meaning that the supramolecular structures have 10-fold long charge carrier lifetime by the incorporation of H-bonds compared to the control. This is translated in faster charge recombination for the control molecule, **HDPPH**.

The UV-Vis spectra of the three derivatives in the solid state were measured on cast thin films from different solvents (Figure S7), showing the appearance of predominant J-aggregate bands in all cases, with a red-shift of approximately 30 nm for the H-bonded derivatives compared to the control. While the spectra on thin film for the H-bonded derivatives is similar to the ones in solution (Figure 1a-b), the spectra differ for the control molecule. This means that on thin film, π - π stacking is guiding the assembly since the J-aggregate band is also present in the control molecule compared to the spectra in solution (Figure 1c). Nevertheless, the only difference among the three molecules is the presence of H-bonds in **HDPPBA-C** and **HDPPBA-N**, which create connections among stacks of DPP derivatives, yielding the superior values of photoconductivity and of charge carrier lifetime.

Additional measurements were performed by extending the time window up to 100 μs and interestingly, the charge carrier lifetime of **HDPPBA-N** was one order of magnitude longer than the

one of **HDPPBA-C**, finding values of 3.7×10^{-5} s and 1.6×10^{-4} s, respectively (Figure 4b and Table 1, entries 4 and 5). These results show that the subtle difference in amide topology plays an important role in the self-assembly process of both derivatives, and thus, in the electrical performance. Furthermore, we have observed that the charge carrier lifetime of the H-bonded structures is extraordinarily long, being at least of one order of magnitude larger than similar H-bonded systems measured by FP-TRMC and reported in the literature.^{16,36} In our case, the amide groups are separated from the π -conjugated segment by a flexible alkyl linker, while in the other examples reported in literature, the amide bonds are directly attached to it. Our future investigations will be focused on elucidating why this particular molecular design results in supramolecular structures with long charge carrier lifetimes.

The higher photoconductivity values and the slower recombination of **HDPPBA-C** and **HDPPBA-N** in comparison to **HDPPH** highlight the beneficial effect of H-bonds in supramolecular electronic systems.

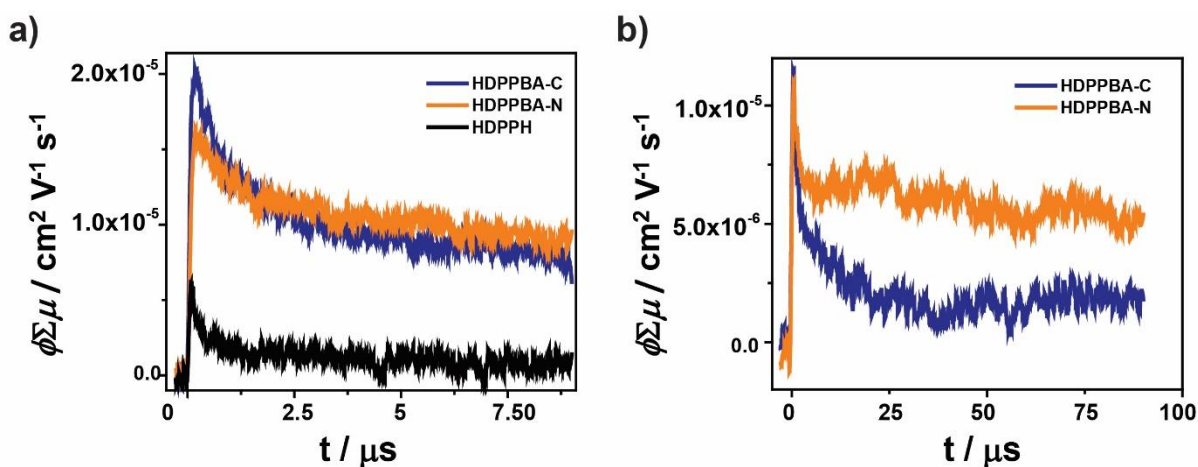


Figure 4. Kinetic traces of photoconductivity transients of **HDPPBA-C**, **HDPPBA-N** and **HDPPH** cast from chloroform/toluene solutions at 2.5 mg/ml. a) Up to 10 μ s and b) Up to 100 μ s.

Table 1. Photoconductivity ($\phi\Sigma\mu$) values, rate constants (k , calculated 3 μ s after pulse excitation) and half lifetime ($t_{1/2}$) values for **HDPPBA-C**, **HDPPBA-N** and **HDPPH**

Entry	Derivative	$\phi\Sigma\mu / \text{cm}^2\text{V}^{-1}\text{s}^{-1}$	k / s^{-1}	$t_{1/2} / \text{s}$
1	HDPPBA-C	2.0×10^{-5}	4×10^4	2×10^{-5}
2	HDPPBA-N	1.6×10^{-5}	3×10^4	2×10^{-5}
3	HDPPH	5.8×10^{-6}	8×10^5	8×10^{-6}
4	HDPPBA-C^a	1.1×10^{-5}	2×10^4	3.7×10^{-5}
5	HDPPBA-N^a	1.1×10^{-5}	0.4×10^4	1.6×10^{-4}

^aMeasured up to 100 μ s

Conclusions

We have synthesized and characterized two different topology amide-containing DPP derivatives and a control analogue without H-bonding units. The differences in self-assembly properties between the C- and N-centered amide topologies have been demonstrated, as well as their distinct charge carrier recombination lifetimes. Interestingly, the comparison to the control molecule has shown one order of magnitude superior photoconductivity for the H-bonded molecules as well as one order of magnitude slower recombination lifetimes, stressing the beneficial role of H-bonding in the charge transport properties of supramolecular systems. Furthermore, we have found out that with this particular molecular design, placing the H-bonding units between two alkyl spacers, longer recombination times are obtained comparing to previously reported supramolecular systems measured by the same technique. These results are very relevant for the future design and implementation of H-bonded semiconductors into electronic devices with long charge carrier lifetimes.

Supporting Information

All the synthetic procedures and additional spectroscopy images can be found in the supporting information.

References

- (1) Yagai, S. Supramolecularly Engineered Functional π -Assemblies Based on Complementary Hydrogen-Bonding Interactions. *Bull. Chem. Soc. Jpn.* **2014**, 31.
- (2) Bialas, D.; Kirchner, E.; Röhr, M. I. S.; Würthner, F. Perspectives in Dye Chemistry: A Rational Approach toward Functional Materials by Understanding the Aggregate State. *J. Am. Chem. Soc.* **2021**, 143 (12), 4500–4518. <https://doi.org/10.1021/jacs.0c13245>.

- (3) Chen, H.; Fraser Stoddart, J. From Molecular to Supramolecular Electronics. *Nature Reviews Materials* **2021**, 1–25. <https://doi.org/10.1038/s41578-021-00302-2>.
- (4) Aida, T.; Meijer, E. W.; Stupp, S. I. Functional Supramolecular Polymers. *Science* **2012**, 335 (6070), 813–817.
- (5) González-Rodríguez, D.; Schenning, A. P. H. J. Hydrogen-Bonded Supramolecular π -Functional Materials. *Chem. Mater.* **2011**, 23 (3), 310–325. <https://doi.org/10.1021/cm101817h>.
- (6) Aytun, T.; Barreda, L.; Ruiz-Carretero, A.; Lehrman, J. A.; Stupp, S. I. Improving Solar Cell Efficiency through Hydrogen Bonding: A Method for Tuning Active Layer Morphology. *Chemistry of Materials* **2015**, 27 (4), 1201–1209. <https://doi.org/10.1021/cm503915t>.
- (7) Ghosh, T.; Panicker, J.; Nair, V. Self-Assembled Organic Materials for Photovoltaic Application. *Polymers* **2017**, 9 (3), 112. <https://doi.org/10.3390/polym9030112>.
- (8) Stone, D. A.; Tayi, A. S.; Goldberger, J. E.; Palmer, L. C.; Stupp, S. I. Self-Assembly and Conductivity of Hydrogen-Bonded Oligothiophene Nanofiber Networks. *Chemical Communications* **2011**, 47 (20), 5702. <https://doi.org/10.1039/c1cc10809c>.
- (9) Xiao, Z.; Sun, K.; Subbiah, J.; Ji, S.; Jones, D. J.; Wong, W. W. H. Hydrogen Bonding in Bulk Heterojunction Solar Cells: A Case Study. *Scientific Reports* **2014**, 4. <https://doi.org/10.1038/srep05701>.
- (10) Kumar, R. J.; Subbiah, J.; Holmes, A. B. Enhancement of Efficiency in Organic Photovoltaic Devices Containing Self-Complementary Hydrogen-Bonding Domains. *Beilstein Journal of Organic Chemistry* **2013**, 9, 1102–1110. <https://doi.org/10.3762/bjoc.9.122>.
- (11) Militzer, S.; Tran, T. M. P.; Mésini, P. J.; Ruiz-Carretero, A. Tuning the Optical and Self-Assembly Properties of Diketopyrrolopyrrole Semicarbazone Derivatives through Hydrogen Bonding. *ChemNanoMat* **2018**, 4 (8), 790–795. <https://doi.org/10.1002/cnma.201800192>.
- (12) Schoonbeek, F. S.; Esch, J. H. van; Wegewijs, B.; Rep, D. B. A.; Haas, M. P. de; Klapwijk, T. M.; Kellogg, R. M.; Feringa, B. L. Efficient Intermolecular Charge Transport in Self-Assembled Fibers of Mono- and Bithiophene Bisurea Compounds. *Angewandte Chemie International Edition* **1999**, 38 (10), 1393–1397. [https://doi.org/10.1002/\(SICI\)1521-3773\(19990517\)38:10<1393::AID-ANIE1393>3.0.CO;2-H](https://doi.org/10.1002/(SICI)1521-3773(19990517)38:10<1393::AID-ANIE1393>3.0.CO;2-H).
- (13) Yao, J.; Yu, C.; Liu, Z.; Luo, H.; Yang, Y.; Zhang, G.; Zhang, D. Significant Improvement of Semiconducting Performance of the Diketopyrrolopyrrole–Quaterthiophene Conjugated Polymer through Side-Chain Engineering via Hydrogen-Bonding. *Journal of the American Chemical Society* **2016**, 138 (1), 173–185. <https://doi.org/10.1021/jacs.5b09737>.
- (14) Ghosh, S.; Li, X.-Q.; Stepanenko, V.; Würthner, F. Control of H- and J-Type π Stacking by Peripheral Alkyl Chains and Self-Sorting Phenomena in Perylene Bisimide Homo- and Heteroaggregates. *Chemistry – A European Journal* **2008**, 14 (36), 11343–11357. <https://doi.org/10.1002/chem.200801454>.
- (15) Ghosh, S.; Cherumukkil, S.; Suresh, C. H.; Ajayaghosh, A. A Supramolecular Nanocomposite as a Near-Infrared-Transmitting Optical Filter for Security and Forensic Applications. *Advanced Materials* **2017**, 29 (46), 1703783. <https://doi.org/10.1002/adma.201703783>.
- (16) Ghosh, S.; Raveendran, R.; Saeki, A.; Seki, S.; Namboothiry, M.; Ajayaghosh, A. Charge Carrier Polarity Modulation in Diketopyrrolopyrrole-Based Low Band Gap Semiconductors by Terminal Functionalization. *ACS Appl. Mater. Interfaces* **2019**, 11 (1), 1088–1095. <https://doi.org/10.1021/acsami.8b16714>.
- (17) Militzer, S.; Nishimura, N.; Ávila-Rovelo, N. R.; Matsuda, W.; Schwaller, D.; Mésini, P. J.; Seki, S.; Ruiz-Carretero, A. Impact of Chirality on Hydrogen-Bonded Supramolecular Assemblies and Photoconductivity of Diketopyrrolopyrrole Derivatives. *Chem. Eur. J.* **2020**, chem.202001540. <https://doi.org/10.1002/chem.202001540>.
- (18) Tevis, I. D.; Tsai, W.-W.; Palmer, L. C.; Aytun, T.; Stupp, S. I. Grooved Nanowires from Self-Assembling Hairpin Molecules for Solar Cells. *ACS Nano* **2012**, 6 (3), 2032–2040. <https://doi.org/10.1021/nn203328n>.
- (19) Ruiz-Carretero, A.; Aytun, T.; Bruns, C. J.; Newcomb, C. J.; Tsai, W.-W.; Stupp, S. I. Stepwise Self-Assembly to Improve Solar Cell Morphology. *Journal of Materials Chemistry A* **2013**, 1 (38), 11674. <https://doi.org/10.1039/c3ta12411h>.

- (20) Huang, C.-H.; McClenaghan, N. D.; Kuhn, A.; Hofstraat, J. W.; Bassani, D. M. Enhanced Photovoltaic Response in Hydrogen-Bonded All-Organic Devices. *Organic Letters* **2005**, 7 (16), 3409–3412. <https://doi.org/10.1021/ol050966l>.
- (21) Huang, C.-H.; McClenaghan, N. D.; Kuhn, A.; Bravic, G.; Bassani, D. M. Hierarchical Self-Assembly of All-Organic Photovoltaic Devices. *Tetrahedron* **2006**, 62 (9), 2050–2059. <https://doi.org/10.1016/j.tet.2005.09.150>.
- (22) Hoeben, F. J. M.; Herz, L. M.; Daniel, C.; Jonkheijm, P.; Schenning, A. P. H. J.; Silva, C.; Meskers, S. C. J.; Beljonne, D.; Phillips, R. T.; Friend, R. H. et al. Efficient Energy Transfer in Mixed Columnar Stacks of Hydrogen-Bonded Oligo (p-Phenylene Vinylene) s in Solution. *Angewandte Chemie* **2004**, 116 (15), 2010–2013.
- (23) *Hydrogen bonding ability of the amide group*. <https://pubs.acs.org/doi/pdf/10.1021/ja00819a013> (accessed 2019-12-22). <https://doi.org/10.1021/ja00819a013>.
- (24) Philips, D. S.; Kartha, K. K.; Politi, A. T.; Krüger, T.; Albuquerque, R. Q.; Fernández, G. Interplay between H-Bonding and Preorganization in the Evolution of Self-Assembled Systems. *Angewandte Chemie International Edition* **2019**, 58 (14), 4732–4736. <https://doi.org/10.1002/anie.201813955>.
- (25) Wegner, M.; Dudenko, D.; Sebastiani, D.; A. Palmans, A. R.; Greef, T. F. A. de; Graf, R.; W. Spiess, H. The Impact of the Amide Connectivity on the Assembly and Dynamics of Benzene-1,3,5-Tricarboxamides in the Solid State. *Chemical Science* **2011**, 2 (10), 2040–2049. <https://doi.org/10.1039/C1SC00280E>.
- (26) Ruiz-Carretero, A.; Roveló, N. R. Á.; Militzer, S.; Mésini, P. J. Hydrogen-Bonded Diketopyrrolopyrrole Derivatives for Energy-Related Applications. *J. Mater. Chem. A* **2019**, 7 (41), 23451–23475. <https://doi.org/10.1039/C9TA05236D>.
- (27) Chandran, D.; Lee, K.-S. Diketopyrrolopyrrole: A Versatile Building Block for Organic Photovoltaic Materials. *Macromol. Res.* **2013**, 21 (3), 272–283. <https://doi.org/10.1007/s13233-013-1141-3>.
- (28) Ghosh, S.; Shankar, S.; Philips, D. S.; Ajayaghosh, A. Diketopyrrolopyrrole-Based Functional Supramolecular Polymers: Next-Generation Materials for Optoelectronic Applications. *Materials Today Chemistry* **2020**, 16, 100242. <https://doi.org/10.1016/j.mtchem.2020.100242>.
- (29) Ghosh, S.; Philips, D. S.; Saeki, A.; Ajayaghosh, A. Nanosheets of an Organic Molecular Assembly from Aqueous Medium Exhibit High Solid-State Emission and Anisotropic Charge-Carrier Mobility. *Advanced Materials* **2017**, 29 (10), 1605408. <https://doi.org/10.1002/adma.201605408>.
- (30) Militzer, S.; Tran, T. M. P.; Mésini, P. J.; Ruiz-Carretero, A. Tuning the Optical and Self-Assembly Properties of Diketopyrrolopyrrole Semicarbazone Derivatives through Hydrogen Bonding. *ChemNanoMat* **2018**, 4 (8), 790–795. <https://doi.org/10.1002/cnma.201800192>.
- (31) Carretero, A. R.; Militzer, S.; Nishimura, N.; Ávila-Roveló, N. R.; Matsuda, W.; Schwaller, D.; Mésini, P. J.; Seki, S. Impact of Chirality on Hydrogen-bonded Supramolecular Assemblies and Photoconductivity of Diketopyrrolopyrrole Derivatives. *Chemistry – A European Journal* **2020**. <https://doi.org/10.1002/chem.202001540>.
- (32) Pop, F.; Humphreys, J.; Schwarz, J.; Brown, L.; Berg, A. van den; Amabilino, D. B. Towards More Sustainable Synthesis of Diketopyrrolopyrroles. *New J. Chem.* **2019**, 43 (15), 5783–5790. <https://doi.org/10.1039/C9NJ01074B>.
- (33) Zhou, Y.; Guzman, C. X.; Helguero-Kelley, L. C.; Liu, C.; Peurifoy, S. R.; Captain, B.; Braunschweig, A. B. Diketopyrrolopyrrole Assembly into J-Aggregates. *Journal of Physical Organic Chemistry* **2016**, 29 (12), 689–699. <https://doi.org/10.1002/poc.3548>.
- (34) McQuade, D. T.; McKay, S. L.; Powell, D. R.; Gellman, S. H. Indifference to Hydrogen Bonding in a Family of Secondary Amides. *J. Am. Chem. Soc.* **1997**, 119 (36), 8528–8532. <https://doi.org/10.1021/ja9711019>.
- (35) Frisch, M. J.; Trucks, G. W.; Schlegel, H. B.; Scuseria, G. E.; Robb, M. A.; Cheeseman, J. R.; Scalmani, G.; Barone, V.; Petersson, G. A.; Nakatsuji, H. Gaussian 16, 2016.
- (36) Ghosh, S.; Das, S.; Saeki, A.; Praveen, V. K.; Seki, S.; Ajayaghosh, A. A Hybrid Organogel of a Low Band Gap Diketopyrrolopyrrole with PC71BM: Phase Separated Morphology and

Acknowledgments

The authors acknowledge the characterization facility for UV/ Vis and FTIR and the microscopy facility of Institute Charles Sadron (CNRS). The authors thank Christian Blanck and Marc Schmutz from the microscopy platform of Institute Charles Sadron (CNRS) for the TEM imaging. A.R.C. and N.R.A.R. thank the Foundation for Frontier Research in Chemistry (FRC) LabEx Emerging Investigators Grant 2018 (CSC-ARC-18). A.R.C. and G.M. thank the Graduate School of Complex Systems Chemistry of Strasbourg for his doctoral fellowship funded by the French National Research Agency (CSC-IGS ANR-17-EURE-0016). The authors thank the Agence Nationale de la Recherche (ANR JCJC TOTALBOND) and the International Emerging Actions CNRS 2020 (SUPRAWAVE).

Conflicts of interest

The authors declare no conflicts of interest